ISSN 1064-2269, Journal of Communications Technology and Electronics, 2011, Vol. 56, No. 6, pp. 699–707. © Pleiades Publishing, Inc., 2011.
Original Russian Text © K.V. Kalashnikov, A.V. Khudchenko, A.B. Baryshev, V.P. Koshelets, 2011, published in Radiotekhnika i Elektronika, 2011, Vol. 56, No. 6, pp. 751–759.

PHYSICAL PROCESSES IN ELECTRON DEVICES

Harmonic Mixer Based on Superconductor–Insulator–Superconductor Tunnel Junction

K. V. Kalashnikov, A. V. Khudchenko, A. B. Baryshev, and V. P. Koshelets

Received January 26, 2010

Abstract—The operation of a harmonic mixer based on a superconductor–insulator–superconductor tunnel junction has been investigated. The dependence of the power of the intermediate-frequency signal on the parameters of the input signals and on the tunnel-junction bias voltage has been determined and experimentally measured. The theoretical and experimental data are in good qualitative and satisfactory quantitative agreement.

DOI: 10.1134/S106422691106009X

INTRODUCTION

The Institute of Radio Engineering and Electronics, Russian Academy of Sciences, and the SRON Netherlands Institute for Space Research jointly proposed and developed a superconducting integrated receiver (SIR) operating in a frequency range of 500 to 650 GHz [1, 2]. This receiver is designed for oblique sounding of the Earth atmosphere from aboard a high-altitude balloon (Terahertz Limb Sounder (TELIS) project) [3]. The first test flight was successfully performed in March 2009. The purpose of the flight was to obtain information on the vertical distribution of the concentration of various atmospheric gases (H_2–^{18}O, HDO, CIO, O_2, isotopes O_3, HCl, and HOCl).

In the SIR, a microchip measuring 4 mm × 4 mm × 0.5 mm combines a low-noise mixer based on a superconductor–insulator–superconductor (SIS) tunnel junction, a quasi-optical antenna; a superconducting flux-flow oscillator (FFO), which acts as a local oscillator and is based on the use of the magnetic-vortex flux flow in a distributed Josephson tunnel junction; and a second SIS harmonic mixer (HM), which is used in the FFO phase-locking system (PLS).

Figure 1 shows a simplified block diagram of a SIR with the FFO phase-locking system. The signal from the FFO and the signal from the observed source received by the antenna are multiplied in the SIS mixer. As a result of the multiplication, the received

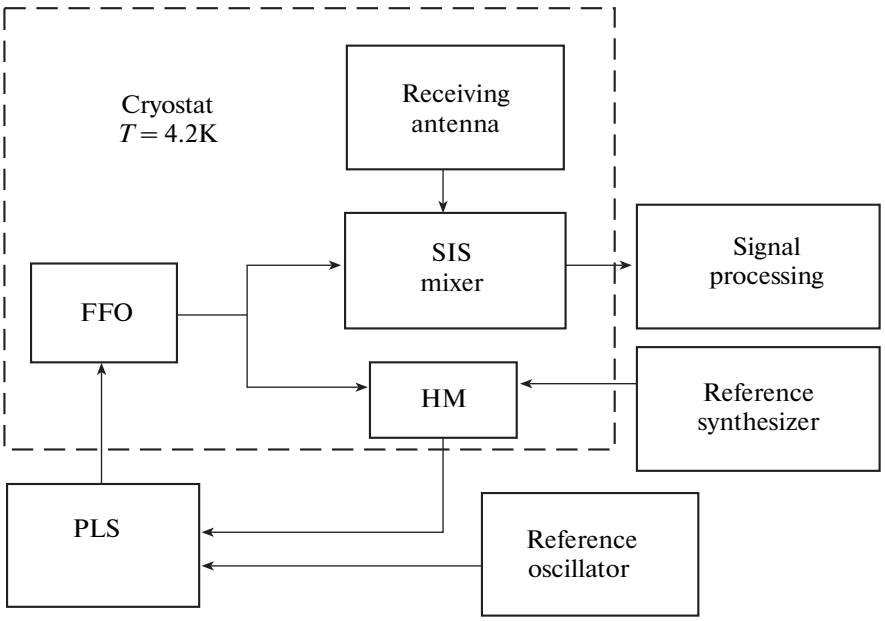

Fig. 1. Simplified block diagram of the SIR.

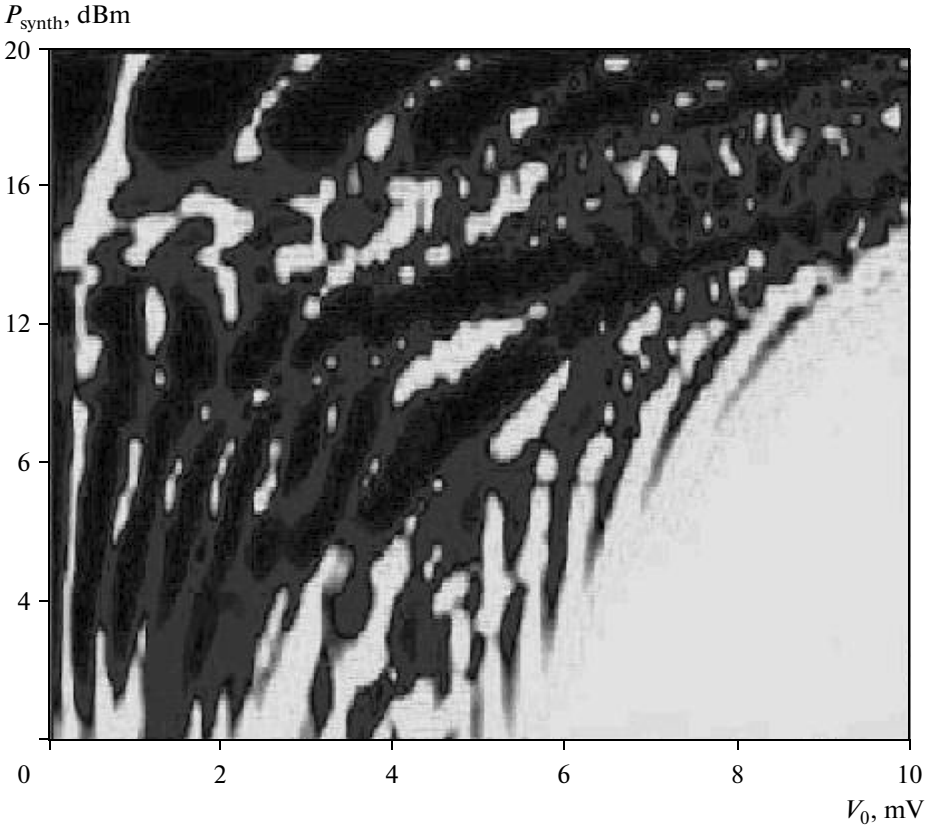

Fig. 2. Typical experimental dependence of the IF-signal power on the bias voltage and on the power of the reference synthesizer ($f_{FFO} = 21$ GHz, $k = 24$).

signal is shifted in frequency into a range of 4 to 8 GHz. It is next delivered first to a "cold" HEMT (high-electron-mobility transistor) amplifier and then to the amplifiers that are outside the cryostat. Part of the FFO power is coupled into the SIS HM, where it is mixed with the kth harmonic of a tunable reference synthesizer (frequencies in a range of 18 to 23 GHz are used). As a result, an intermediate-frequency (IF) signal with the frequency

$$f_{IF} = \pm (f_{FFO} - kf_{SYNTH}). \quad (1)$$

is produced, which is used in the PLS.

The PLS provides phase locking between the FFO and the reference oscillator. This system is required for improving the oscillator stability and oscillator spectral characteristics, which determine the SIR spectral characteristics [4].

In order for the PLS operation to be effective and stable, the power of the HM output signal must be sufficiently high. Such a signal is considerably greater than the noise of the IF signal, which is determined by the amplifiers and the HM itself, and provides high signal-to-noise ratio. It was found experimentally that the magnitude of the IF signal strongly varies as the HM bias voltage is changed and that its dependence on the power and frequency of the signals applied to the HM is a complex one [3]. A typical dependence of IF-signal power P_{IF} on HM bias voltage V_0 and on power of the reference synthesizer P_{synth} is shown in Fig. 2. The change in color from light to dark corresponds to an increase in P_{IF}. Until recently, no theory explaining the presented pattern was proposed.

Study [5] describes the use of the SIS junction as a subharmonic mixer for a heterodyne receiver using harmonics with small numbers ($k = 2–5$). In study [6], the use of a SIS-junction HM employing harmonics with numbers $k > 30$ in antenna-pattern measurement is described. In the present study, dependences of the power of the HM output signal on the bias voltage that are measured at various power levels of the RF signal are presented. This study is dedicated to the theoretical description and simulation of the operation of the SIS-junction HM and to its experimental investigation aimed at validation of the theoretical results. This investigation is necessary for the understanding of the HM properties, for the efficient use of the HM in cryogenic devices, and, in particular, for maximization of the IF output signal.

1. THEORETICAL DESCRIPTION OF THE SIS-JUNCTION HARMONIC MIXER

The main purpose of the HM calculation is to determine the dependence of the IF output signal on

the parameters of the applied signals and on the SIS-junction bias voltage.

A detailed theoretical description of the operation of the SIS junction under the action of RF signals is given in [7–9]. However, simplifying assumptions that the applied signals are small and that the junction capacitance shunts the higher harmonics of the reference synthesizer are made in study [7]. In studies [8, 9], a procedure for describing the SIS junction is given for a general case that the powers of the applied signals may assume arbitrary values. The presented model is the most complete one to date. With this model, the self-consistent problem for the SIS junction placed in the external circuit is solved and certain characteristics of the SIS-junction HM are calculated [9].

The present study describes the HM on the basis of a simplified and clearer theory, which is an extension of study [10] to the case of several signals applied to the tunnel junction. This theory ignores the effect of the external circuit on the pumping of the SIS junction. However, this model yields qualitatively true and quantitatively satisfactory results that agree with the results of study [9]. This fact indicates that the model takes into account the main factors that determine the generation of the HM output signal.

Let us consider a model of weakly-interacting quasiparticles without considering the spin effects caused by the action of the electric field, which is similar to the model presented in study [10].

The wave function of a quasiparticle with energy E with no alternating electric field applied has the form $\Psi = f(x,y,z)\exp(-iEt/\hbar)$, where $f(x,y,z)$ is a certain coordinate function, i is the imaginary unit, t is the time, and $\hbar$ is the Planck constant. This wave function is the eigenfunction of unexcited-system Hamiltonian $\hat{H}_0$. When two periodic signals are applied to the electrodes of the SIS junction, the junction voltage is $V_{\omega 1}\cos(\omega_1 t) + V_{\omega 2}\cos(\omega_2 t)$, where ω_1 and ω_2 are the circular frequencies of the first and second signals, respectively. In this case, the Hamiltonian of the system of quasiparticles is written as $\hat{H} = \hat{H}_0 + eV_{\omega 1}\cos(\omega_1 t) + eV_{\omega 2}\cos(\omega_2 t)$, where $\hat{H}_0$ is the Hamiltonian an unexcited system, $\hat{H}$ is the Hamiltonian of a system under the action of two harmonic signals, and e is the electron charge. We will seek the new wave function in the form

$$\Psi = f(x,y,z) \times \exp(-iEt/\hbar)\left(\sum_n B_n \exp(-in\omega_1 t)\right) \times \left(\sum_m C_m \exp(-im\omega_2 t)\right),$$

where B_n and C_m are unknown functions.

Substitution of the wave function into the Schr@odinger equation $i\hbar\frac{\partial\psi}{\partial t} = \hat{H}\psi$, gives the equations for B_n and C_m:

$$2nB_n = \frac{eV_1}{\hbar\omega_1}(B_{n+1} + B_{n-1}),$$

$$2mC_m = \frac{eV_2}{\hbar\omega_2}(C_{m+1} + C_{m-1}).$$

By solving these equations, we find

$$B_n = J_n\left(\frac{eV_1}{\hbar\omega_1}\right),$$

$$C_m = J_m\left(\frac{eV_2}{\hbar\omega_2}\right),$$

where $J_i(x)$ is the Bessel function of order i.

Thus, the solution to the Schr@odinger equation is the wave function

$$\Psi = f(x)\exp(-iEt/\hbar)\left(\sum_n\sum_m J_n\left(\frac{eV_{\omega 1}}{\hbar\omega_1}\right)J_m\left(\frac{eV_{\omega 2}}{\hbar\omega_2}\right) \times \exp\left[-i(n\omega_1 + m\omega_2)t\right]\right). \quad (2)$$

The energy levels of the quasiparticles are thus seen to be split into the levels described by wave functions Ψ_{nm} with energies $E + n\hbar\omega_1 + m\hbar\omega_2$; $n, m = 0, \pm1, \pm2\ldots$, and, accordingly, with the level-occupation probabilities that are proportional to $J_n\left(\frac{eV_{\omega 1}}{\hbar\omega_1}\right)J_m\left(\frac{eV_{\omega 2}}{\hbar\omega_2}\right)$.

The quasiparticle tunnel current occurs when quasiparticles pass from one SIS-junction electrode to the other. When a DC voltage is applied, this current is described by complex current-response function $j(V)$, which is calculated in study [11] and has the form $j(V) = iI_{dc}(V) + I_{KK}(V)$ (Fig. 3). Here, $I_{dc}(V)$ is the voltage–current characteristic (VCC) of the SIS junction and function $I_{KK}(V)$ is related to $I_{dc}(V)$ by the Kramers-Kronig relationship.

Note that, in the calculation, function $I_{dc}(V)$ is taken from the experimental data rather than from computed results. Thus, all information on the gap voltage and the current jump at the gap voltage is contained in the HM VCC.

On absorption of a radiation quantum, the quasiparticle increases its energy by $\hbar\omega$, which is equivalent to application of voltage $\hbar\omega/e$ to the junction. In this case, the tunnel current is determined by function $j(V + \hbar\omega/e)$. Since the quasiparticle can simultaneously absorb several photons with energies $\hbar\omega_1$ and $\hbar\omega_2$, the total tunnel current can be found by summation of the current-response functions

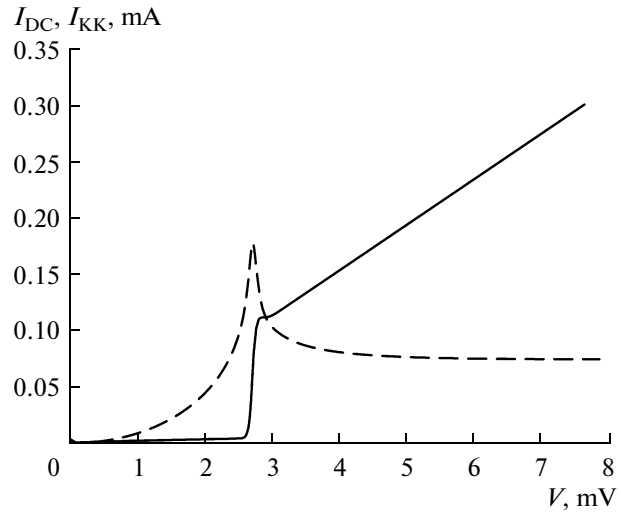

Fig. 3. Current-response function $j(V)$ used in the calculation: (solid line) imaginary part and (dashed line) real part.

$j_{nm} = j\left(V + \frac{n\hbar\omega_1}{e} + \frac{m\hbar\omega_2}{e}\right)$ with the probability of the quasiparticle tunneling taken into account. The probability of a transition of the quasiparticle that is in state Ψ_{nm} into state Ψ_{lk} is determined by matrix element $\langle\Psi_{nm}|\Psi_{lk}\rangle$, where

$$|\Psi_{nm}\rangle = f(x)\exp(-iEt/\hbar) \times \left(J_n\left(\frac{eV_{\omega 1}}{\hbar\omega_1}\right)J_m\left(\frac{eV_{\omega 2}}{\hbar\omega_2}\right)\exp[-i(n\omega_1 + m\omega_2)t]\right),$$

$$\langle\Psi_{lk}| = g(x)\exp(iEt/\hbar) \times \left(J_l\left(\frac{eV_{\omega 1}}{\hbar\omega_1}\right)J_k\left(\frac{eV_{\omega 2}}{\hbar\omega_2}\right)\exp[i(l\omega_1 + k\omega_2)t]\right).$$

In order for the total junction current to be found, it is necessary to sum such matrix elements over various n, m, l, and k:

$$I(V,t) = \mathrm{Im}\sum_n\sum_m\sum_l\sum_k J_n(\alpha_1)J_l(\alpha_1)J_m(\alpha_2)J_k(\alpha_2) \times \exp[-i((n-l)\omega_1 + (m-k)\omega_2)t]\, j\left(V + \frac{n\hbar\omega_1}{e} + \frac{m\hbar\omega_2}{e}\right).$$

Performing summation-index change $(n - l \to l; m - k \to k)$, we obtain the formula

$$I(V,t) = \mathrm{Im}\sum_n\sum_m\sum_l\sum_k J_n(\alpha_1)J_{n+l}(\alpha_1)J_m(\alpha_2) \times J_{m+k}(\alpha_2)\exp[-i(l\omega_1 + k\omega_2)t]\, j\left(V + \frac{n\hbar\omega_1}{e} + \frac{m\hbar\omega_2}{e}\right), \quad (3)$$

where $\alpha_i = \frac{eV_{\omega i}}{\hbar\omega_i}$.

Note that function (3) can be written as

$$I(V,t) = a_0 + \sum_{l=0}^{\infty *} \times \sum_{k=0}^{\infty *}\left(2a_{lk}\cos((l\omega_1 + k\omega_2)t) + 2b_{lk}\sin((l\omega_1 + k\omega_2)t)\right), \quad (4)$$

where a_0 is the term of the sum corresponding to $l = 0, k = 0 = 0$. The asterisk marking the summation symbols indicates that summation is performed over l and k that are not simultaneously zero.

Thus, as it follows from formula (3), when two signals are applied to the SIS junction, we obtain output signals at all frequencies that can be defined by the formula $l\omega_1 + k\omega_2$, where l and k are the integers. Of practical importance is the case of the HM, namely: the case where frequency of the first signal is close to the multiple frequency of the second signal, i.e., $\omega_1 - k\omega_2 \ll \omega_2$. For convenience of notation, we assume here that $\omega_1 \equiv 2\pi f_{RF}$ and $\omega_2 \equiv 2\pi f_{synth}$. In this case, at the intermediate frequency $f_{IF} = f_{RF} - kf_{synth}$, the current amplitude can be written as

$$I_{IF} = \sqrt{a_{1k}{}^2 + b_{1k}{}^2}, \quad (5)$$

where

$$a_{1k}(V) = \sum_{n,m} J_n(\alpha_1)J_m(\alpha_2)\left[J_{n+1}(\alpha_1)J_{m-k}(\alpha_2) + J_{n-1}(\alpha_1)J_{m+k}(\alpha_2)\right] I_{dc}\left(V + \frac{n\hbar\omega_1}{e} + \frac{m\hbar\omega_2}{e}\right),$$

$$b_{1k}(V = \sum_{n,m} J_n(\alpha_1)J_m(\alpha_2)\left[J_{n+1}(\alpha_1)J_{m-k}(\alpha_2) - J_{n-1}(\alpha_1)J_{m+k}(\alpha_2)\right] I_{KK}\left(V + \frac{n\hbar\omega_1}{e} + \frac{m\hbar\omega_2}{e}\right).$$

Formula (5) describes the sought dependence of the current amplitude at intermediate frequency f_{IF} on the frequencies and power levels of the RF signal and the synthesizer signal and, therefore, is the main theoretical result of this section.

2. EXPERIMENTAL MEASUREMENT OF THE CHARACTERISTICS OF THE SIS-JUNCTION HARMONIC MIXER

The experimental data given in [3, 5, 6] are insufficient for verification of the theoretical results. Therefore, an experiment was conducted to measure the magnitude of the output signal of the SIS-junction HM as a function of the power levels of the input signals and of the HM bias voltage $P_{IF}(V_0, P_{synth})$, i.e., to obtain the patterns similar to the patterns shown in Fig. 2.

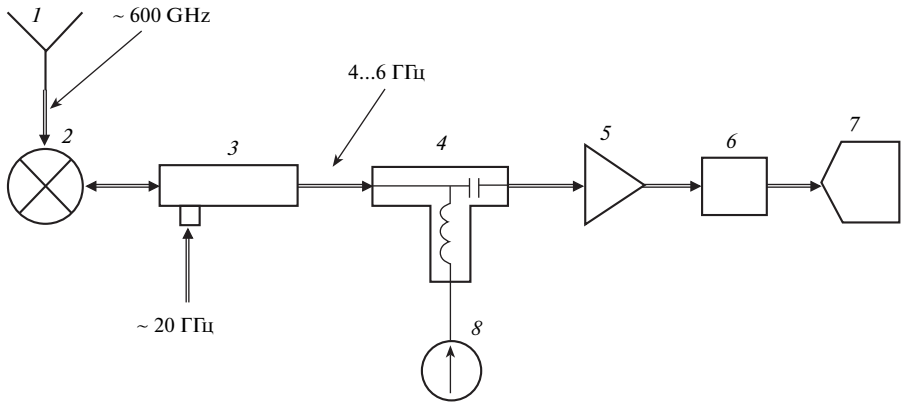

Fig. 4. Experimental setup for measuring the characteristics of the SIS-junction HM: (*1*) antenna; (*2*) HM, (*3*) directional coupler; (*4*) SIS-junction bias tee; (*5*) system of amplifiers; (*6*) bandpass filter; (*7*) power meter; and (*8*) current source, which allows the SIS-junction bias voltage to be set.

In the experiment, we used a single SIS junction made as a Nb–AlO_x–Nb film structure with a surface area of 1 μm^2. The normal resistance of the junction is about 25 Ω, and the gap voltage is 2.8 mV.

In measuring the characteristics of the SIS-junction HM that are determined by the quasiparticle tunneling, the Josephson component of the current was suppressed by the external magnetic field. This circumstance makes the difference between this case and the case represented in Fig. 2. It was found experimentally that the critical current strongly affects the pattern of dependence $P_{IF}(V_0,P_{synth})$. The current instability and variation from experiment to experiment change the $P_{IF}(V_0,P_{synth})$ pattern. However, these critical-current variations do not change the position of the large peaks seen in the upper part of Fig. 2.

The experimental setup is shown in Fig. 4. The SIS junction (*2*) and the antenna (*1*) are placed in a bath cryostat at a liquid-helium temperature of 4.2K. The frequency of the signal arriving at the antenna is of the order of 600 GHz. This signal is generated as the signal from the synthesizer with a frequency of about 25 GHz passes via a superlattice multiplier operating at the 27@th[roman] harmonic. The signal from the reference synthesizer with a frequency of about 20 GHz is applied via the –20dB port of a directional coupler (*3*). The mixer output signal with a frequency of 4–6 GHz is transmitted via the directional coupler (*3*) and via the element for setting the DC bias current of the SIS junction (*4*) and is applied to the input of a system of IF amplifiers (*5*). Next, this signal passes via a narrowband filter (*6*) with a passband of 30 MHz and arrives at a power meter (*7*). The bias current is set by a control unit (*8*). In the measurements, the automatic integrated receiver test and control (IRTECON) system was used [12].

3. COMPARISON AND ANALYSIS OF THE THEORETICAL AND EXPERIMENTAL RESULTS

Prior to comparing the theoretical and experimental results, the RF-signal power was calibrated from the levels of the SIS-junction pumping produced by the RF signal. The calibration was performed as follows. The RF signal alone was applied to the HM, and next the current jump was measured at an SIS-junction bias voltage of 2.5 mV. Next, from the computational results, coefficient $\alpha_1$was selected that provided a calculated junction pumping that agrees with the experimentally measured one.

A separate calibration of reference-signal power P_{synth} was not performed. Quantity P_{synth} characterizes the output power of the generator rather than the power of the signal arriving at the junction, which is decreased by 20 dB in the directional coupler (*3*) (Fig. 4) and is lost in the connecting cables. Theoretical dependences $P_{IF}(V_0,P_{synth})$ were shifted by a constant along the P_{synth} axis until they coincided with the experimental ones.

On calibration, the experimental and calculated dependences $P_{IF}(V_0,P_{synth})$, which are presented in Fig. 5, were analyzed. A comparison between the dependences shows that the calculated patterns are in general agreement with the experimental ones. It should be noted that the synthesizer-power dynamic ranges coincide very closely. The $P_{IF}(V_0,P_{synth})$ pattern is a complex one and resembles an interference pattern. In the case of an RF frequency of 635 GHz (presented in Fig. 5), two bundles of lines are seen at low values of power P_{synth}. The centers of the bundles are located symmetrically about the gap voltage and approach it as frequency f_{RF} decreases. The frequency and the number of lines in the bundle linearly increase with the harmonic number, i.e., as synthesizer frequency f_{synth} decreases. At the base of the bundle, the lines are vertical and the separation of the lines is

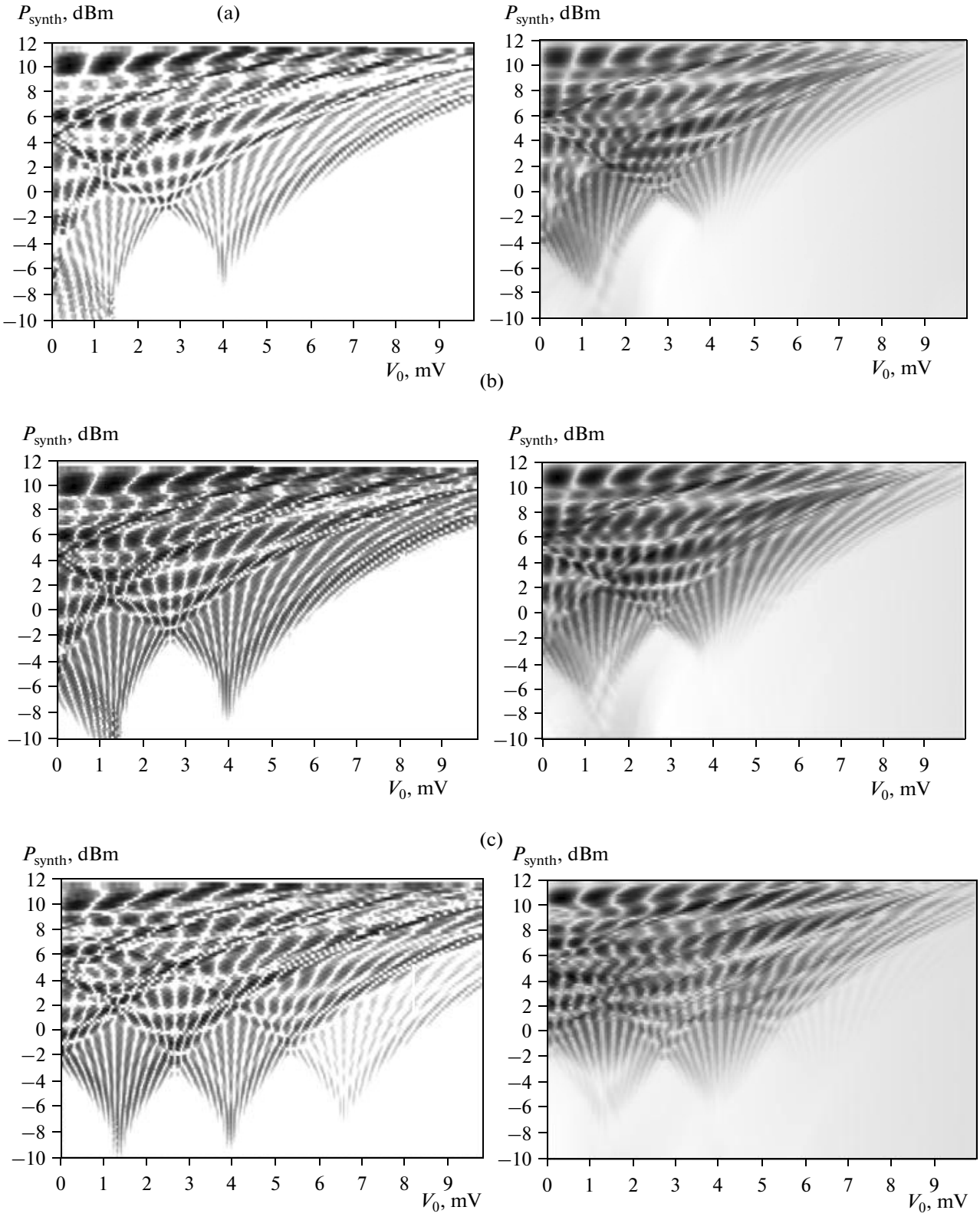

Fig. 5. Experimental (at the left) and theoretical (at the right) dependences $P_{IF}(V20, P_{synth})$ for different RF-signal powers: RF-signal pumping is (a) 15%, (b) 30%, and (c) 55% of the current jump at the gap voltage; f_{RF} = 635 GHz and f_{synth} = 18 GHz, 35th harmonic. The output-signal dynamic scale range is 22 dB.

$2f_{synth}/k_J$, where k_J is the Josephson constant, which is 483.6 GHz/mV, a value that corresponds to the width of the quasiparticle jump on the HM VCC pumped by the synthesizer signal. At higher values of P_{synth}, the bundle lines intersect and form a system of peaks whose separation increases as P_{synth} increases.

The presence of the critical current strongly affects the $P_{IF}(V_0,P_{synth}$ pattern at small values of P_{synth} and makes the observation of the bundles of lines impossible. However, at higher level of applied power P_{synth}, the effect of the critical current is suppressed and the wide peaks are observed regardless of the presence of the critical current. The upper boundary of the presented $P_{IF}(V_0,P_{synth})$ patterns is determined by the fact that, for the junction used, a further increase in P_{synth} in the experiment results in a sharp decrease in the power of the HM output signal.

By constructing the section of the 3D $P_{IF}(V_0,P_{synth})$ pattern for fixed specified power P_{synth}, we obtain $P_{IF}(V_0,P_{synth}$ dependences that are similar to the experimental and theoretical dependences obtained in [6] and [9], respectively (Fig. 6).

An analysis of the behavior of the $P_{IF}(V_0,P_{synth})$ pattern under changes in harmonic number k at the same powers of the RF signals and synthesizer signals shows that, at a zero bias, a maximum power of the IF signal is observed for an even harmonic and a minimum power for an odd harmonic. This result agrees with the experiment and is illustrated in Figs. 7a and 7b, which correspond to $k = 34$ and $k = 35$. This specific behavior of the IF signal at $V_0 = 0$ follows from the analysis of Eq. (5). At a zero bias voltage, we have

$$V_0 = 0;$$
$$J_{-n}(\alpha) = (-1)^n J_n(\alpha);$$
$$I_{DC}(-V) = -I_{DC}(V);$$
$$I_{KK}(-V) = I_{KK}(V).$$

By splitting the sum in (5) into four sums with positive and negative n and m, we find

$$I_{IF}(k) = A(1 + (-1)^k),$$

where A is a certain function of the frequencies and powers of the signals applied to the junction. Thus, at odd k, the IF signal becomes zero and at even k it is positive. This is an important result, since, for certain applications, it is convenient to have a capability of operation at a zero bias voltage by selecting the appropriate synthesizer frequencies.

The 3D $P_{IF}(V_0,P_{synth}$ pattern allows the values of parameters V_0 and P_{synth} needed for setting the system to the operating point to be determined. However, the peaks have different maximum IF-signal powers, which also depend on the value of RF-signal power

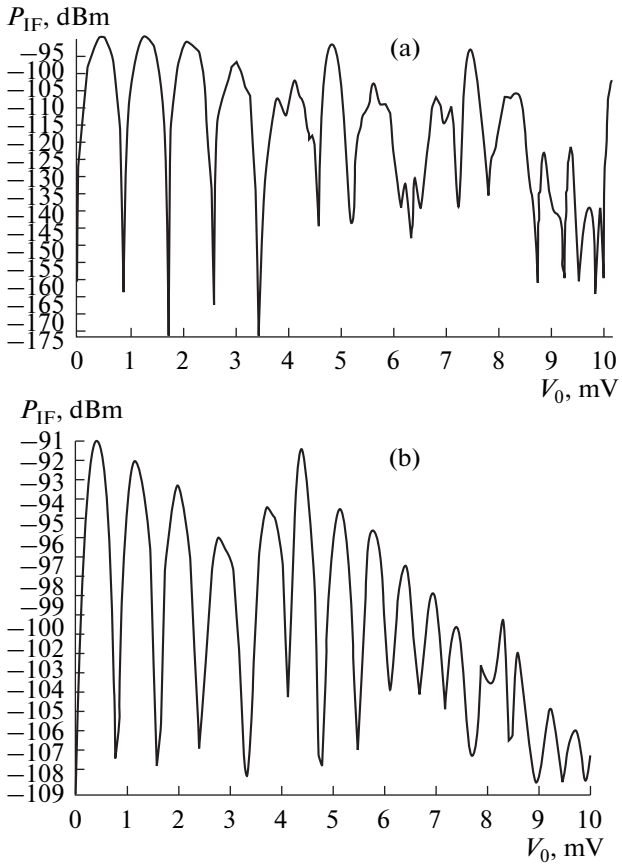

Fig. 6. Section of the dependence shown in Fig.5b made at a level of 10.5 dBm: (a) calculation and (b) experiment.

P_{RF}. The investigation of theoretical dependences $P_{IF}(P_{RF})$ shows that, for each separate peak, there is an optimum value of power P_{RF} at which quantity P_{IF} achieves its maximum. This can be seen in Fig. 8, where dependence $P_{IF}(P_{RF})$ is shown. This dependence is calculated at fixed V_0 and P_{synth}, which corresponds to the peak marked with a cross in Fig. 7b. It can be seen that as P_{RF} increases, the output signal is linearly increased, i.e., the HM operates in a linear mode. It is this mode that was used in study [6] in measuring the antenna pattern. As P_{RF} is increased, the IF signal achieves its maximum and next noticeably decreases as P_{RF} is further increased. The P_{RF} peak point corresponds to the HM pumping (the current at a 2.5-mV junction bias) by a RF signal that is about 30% of the current jump at the gap voltage. It follows from Fig. 6 that, for a Nb–AlO_x–Nb SIS junction with a surface area of 1 μm^2 and a gap-voltage current jump of about 100 μA, at $f_{RF} = 635$ GHz and $f_{synth} = 18$ GHz (the 35th harmonic), the output signal may achieve, according to the calculations, −85 dBm. Experimentally, a value of about −90 dBm was obtained.

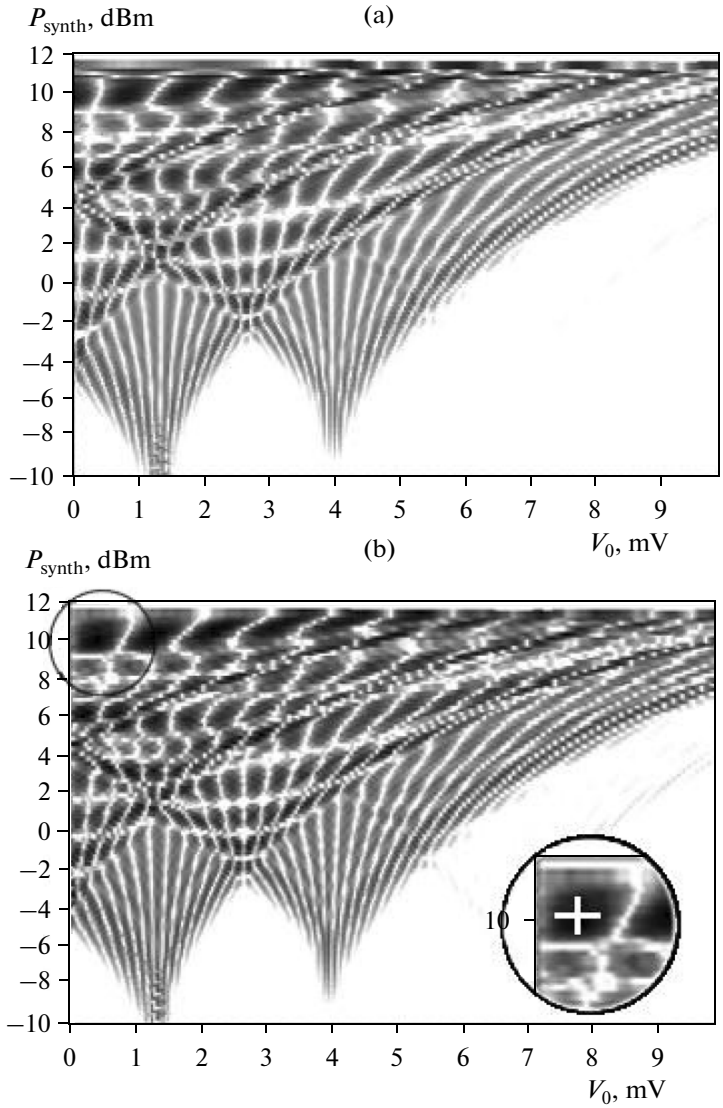

Fig. 7. Theoretical dependences $P_{IF}(V_0,P_{synth})$ for different synthesizer-harmonic numbers at f_{RF} = 635 GHz: F_{synth} = (a)18.53 GHz, 34 th harmonic and (b) 18 GHz, 35th harmonic. Marked with a cross in the insert in Fig. 7b is the point for which Fig. 8 is constructed.

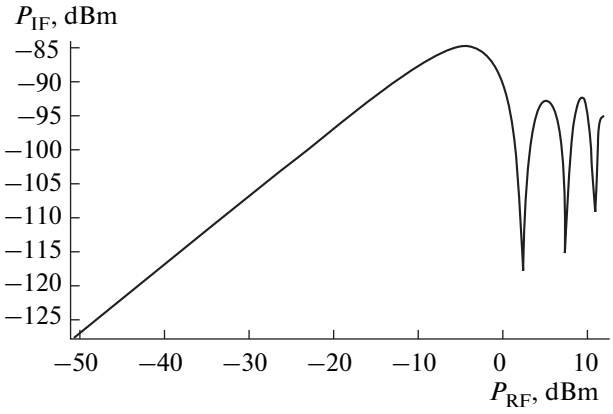

Fig. 8. Theoretical dependence of the IF-signal power on the RF-signal power for V_0,P_{synth} marked with a cross in the insert in Fig. 7b. The peak of the curve corresponds to the RF-signal-pumping current that is equal to a third of the current jump at the gap voltage.

CONCLUSIONS

In the present study, an HM based on a tunnel SIS junction has been theoretically investigated. In order to verify the obtained results, a series of experiments has been conducted. A comparison of the experimental and theoretical results shows that they are in good qualitative and satisfactory quantitative agreement. The dependence of the harmonic SIS mixer on the bias voltage and the magnitude of the applied signals has been analyzed. The behavior of the IF signal at a zero bias voltage has been theoretically explained. The power of the RF signal required for the maximization of the IF signal has been estimated.

ACKNOWLEDGMENTS

We are grateful to Meno Van den Bent for help in the preparation of the experiment.

This study was supported by the Russian Foundation for Basic Research, project nos. 09-02-00246 and 09-02-12172-ofi_m, by the Grant Council of the President of the Russian Federation under the State Program for the support of leading scientific schools of the Russian Federation, grant NSh-5423.2010.2, and by State Contract no. 02.740.11.0795.

REFERENCES

1. V. P. Koshelets and S. V. Shitov, Superconductor Science and Technology **13** (5), R53 (2000).
2. V. P. Koshelets, S. V. Shitov, L. V. Filippenko, et al., Appl. Phys. Lett. **68**, 1273 (1996).
3. V. P. Koshelets, S. V. Shitov, A. B. Ermakov, et al., IEEE Trans. Appl. Supercond. **15**, 960 (2005).
4. V. P. Koshelets and A. V. Khudchenko, Radiotekh. Elektron. (Moscow) **51**, 633 (2006) [J. Commun. Technol. Electron. **51**, 596 (2006)].
5. V. Yu. Belitsky, I. L. Serpuchenko, M. A. Tarasov, and A. N. Vystavkin, in *Proc. Int. Conf. on Millimeter Wave and Far-Infrared Technology (ICMWFT-89), Beijing, Jun. 19–23, 1989* (IEEE, New York, 1989), p. 268.
6. A. Baryshev, M. Carter, R. Hesper, et al., in *Proc, 13th Int. Symp. on Space Terahertz Technology, Harvard, 26–28 Mar. 2002* (Harvard-Smithsonian Center for Astrophysics, Harvard, 2002), p.551.
7. J. R. Tucker and M. J. Feldman, Rev. Mod. Phys. **57**, 1055 (1985).
8. S. Withington, P. Kittara, and G. Yassin, J. Appl. Phys. **93**, 9812 (2003).
9. P. Kittara, S. Withington, and G. Yassin, J. Appl. Phys. **101**, 024508 (2007).
10. P. K. Tien and J. P. Gordon, Phys. Rev. **129**, 647 (1963).
11. N. R. Werthamer, Phys. Rev. **147**, 255 (1966).
12. A. B. Ermakov, S. V. Shitov, A. M. Baryshev, et al., IEEE Trans. Appl. Supercond. **11**, 840 (2001).